Applied Catalysis B: Environmental 191 (2016) 192–201

Contents lists available at ScienceDirect

Applied Catalysis B: Environmental

journal homepage: www.elsevier.com/locate/apcatb

TiO_2 encapsulated in Salicylaldehyde-NH_2-MIL-101(Cr) for enhanced visible light-driven photodegradation of MB

Xiyi Li [1], Yunhong Pi [1], Qibin Xia, Zhong Li, Jing Xiao *

School of Chemistry and Chemical Engineering, and Key Laboratory of Enhanced Heat Transfer and Energy Conservation of the Ministry of Education, South China University of Technology, Guangzhou 510640, China

ARTICLE INFO

Article history:
Received 29 January 2016
Received in revised form 13 March 2016
Accepted 15 March 2016
Available online 16 March 2016

Keywords:
Salicylaldehyde
TiO_2
NH_2-MIL-101(Cr)
Photocatalytic degradation
MB

ABSTRACT

An effective visible light-driven photocatalyst of TiO_2 encapsulated in modified MOF was synthesized for the first time and the resulting TiO_2@Salicylaldehyde-NH_2-MIL-101(Cr) (namely LP(Ti)) was characterized. Then the photodegradation of MB with LP(Ti) was tested. The introduction of salicylaldehyde significantly enhanced the light-absorption properties of LP and LP(Ti), undergoing redshift compared with NH_2-MIL-101(Cr) and TiO_2@NH_2-MIL-101. The LP(Ti) showed an excellent photodegradation efficiency of MB as high as 86% in 60 min of visible-light irradiation with only 5 mg photocatalyst, which was the highest among the tested samples NH_2-MIL-101(Cr), TiO_2@NH_2-MIL-101(Cr), LP, LP(Ti) and Degussa P-25. The LP(Ti)/visible/H_2O_2 system showed the enhanced synergy index by 106%. The mechanism of the photodegradation of MB with H_2O_2 over LP(Ti) under the visible light was further illustrated. This work provides a new approach to design MOF encapsulated TiO_2 for visible light-induced photodegradation of organic contaminants for the environmental remediation.

1. Introduction

The desire of using solar energy to eliminate the organic pollutants makes photocatalysis a potential technology for solving environmental issues confronting mankind. Since the discovery of the first artificial photocatalytic system for pollutants degradation over TiO_2, many metal oxides and sulfides including ZnO, WO_3, CdS, ZnS have been identified as active photocatalysts for photodegradation of organic pollutants in gas or aqueous phase [1–7]. The quantum yield and solar energy conversion efficiency of these developed photocatalysts, however, are still low at present, thus limiting their practical applications in environmental purification. Consequently, it is of great interest to search for new photocatalysts with improved activities.

Metal–organic frameworks (MOFs) are crystalline hybrid inorganic/organic solids with extended structures which can be utilized in many fields, such as gas separation and storage, sensors, and drug delivery [8–10]. Especially, MOFs behave as semiconductors when exposed to light, thus making MOFs potentially be heterogeneous photocatalysts for environmental purification due to their high crystallinity with well-defined pore properties, high specific surface area and tailorable structures [11–14]. Garcia et al. firstly proposed MOF-5 to be an active photocatalyst for photodegradation of phenol. In contrast to a conventional photocatalyst of metal oxide or sulfide, MOF-5 displayed the reverse shape-selectivity in which small phenolic molecules that can diffuse freely into the micropores of MOF-5 are degraded more slowly than those that cannot access to the interior of MOF-5 [15]. Natarajan et al. used different MOFs based on Co, Ni, and Zn as photocatalysts to degrade organic dyes. The photocatalytic results show that all three MOFs are active for the photodegradation of four widely used dyes (orange G, rhodamine B, Remazol Brilliant Blue R, and methylene blue) in the textile industry. However, established MOFs have relatively low photocatalytic activity due to their limited selections of metals and organic ligands [16]. In order to further enhance the catalytic activity, post-synthetic modification (PSM), defined as the chemical derivatization of MOFs after their formation, becomes a practical and powerful tool to generate MOF-based heterogeneous catalysts with improved photocatalytic performance [17,18].

MIL-101 discovered by Férey et al. shows a rigid zeotype cubic structure, which defines nanocages of about 2.9 and 3.4 nm with windows of 1.2 and 1.6 nm, respectively [19]. NH_2-MIL-101(Cr) retains the features of MIL-101, in which amino groups are introduced into the organic frames of the MOF lattice [20]. NH_2-MIL-101(Cr) can be a good candidate for PSM due to its large pores, good thermal stability as well as excellent chemical stability to water and common organic solvents [21]. Moreover, the reactive amino groups existing on the surface of the NH_2-MIL-101(Cr) pores can provide versatility to covalently attach functional species.

* Corresponding author.
E-mail address: cejingxiao@scut.edu.cn (J. Xiao).
[1] These two authors contributed equally to this work.

http://dx.doi.org/10.1016/j.apcatb.2016.03.034
0926-3373/

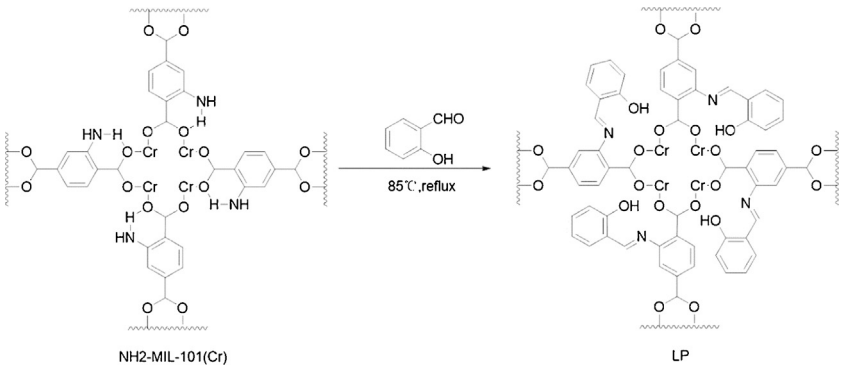

Scheme 1. The reaction between NH_2-MIL-101(Cr) and salicylaldehyde.

Efforts for the PSM strategy of various Cr-MIL-101-NH_2, such as urea-derived MIL-101 by introducing ethyl isocyanate [20,22] and photo-switchable MIL-101 by installing an azo functionality [20], have been achieved successfully. However, the PSM strategy of NH_2-MIL-101(Cr) in the photocatalytic reaction has received few attention up to date.

Herein, a novel photocatalyst of TiO_2 encapsulated in Salicylaldehyde-NH_2-MIL-101 was developed for effective photocatalytic degradation of the organic dye MB under visible-light. High surface area and structure-stable NH_2-MIL-101(Cr) was chosen as a base matrix, and salicylaldehyde was introduced as the linking agent to afford a Schiff base moiety in the porous matrix, which extended the conjugate chain to some extent. Thus it provided a unique environment for the encapsulation of TiO_2. The resulting TiO_2@Salicylaldehyde-NH_2-MIL-101(Cr) (namely LP(Ti)) was characterized by FT-IR, XRD, EDS, nitrogen adsorption/desorption, XPS and UV–vis DRS spectroscopy. The photocatalytic degradation experiments were carried out in a batch reactor. The pronounced impact of introduced phenol group in NH_2-MIL-101(Cr) on the MB photodegradation was investigated. The photodegradation conditions, including pH and the amount of H_2O_2 were optimized. The synergistic effect of LP(Ti)/visible/H_2O_2 was calculated and further discussed. The mechanism for the MB degradation on LP(Ti)/visible/H_2O_2 system was illustrated. The developed new LP(Ti) solid photocatalyst showed high photocatalytic activity, easy recovery and excellent recycling stability for the degradation of MB dye, which may provide a new approach for visible light-induced photodegradation of organic contaminants for the environmental remediation.

2. Experimental

2.1. Materials

Chromic nitrate hydrate (99%, $Cr(NO_3)_3{\cdot}9H_2O$), 2-aminoterephthalic acid (99%), sodium hydroxide (NaOH), *N*,*N*-dimethyl-formamide (DMF), salicylaldehyde (99%), tetrabutyl titanate (99%), H_2O_2 (30%, v/v), methylene blue (MB), hydrochloric acid (HCl) were purchased from Alfa Aesar. Methanol (MeOH) and ethanol (EtOH) was obtained from HPLC. All chemicals used in this study were of commercially available analytical grade and used without further purification.

2.2. Preparation of TiO_2@Salicylaldehyde-NH_2-MIL-101(Cr) solid photocatalyst

2.2.1. Preparation of NH_2-MIL-101(Cr)

NH_2-MIL-101(Cr) was prepared by a mild solvothermal process [23]. Typically, 3.2 g of $Cr(NO_3)_3{\cdot}9H_2O$ and 1.44 g 2-aminoterephthalic acid were added slowly into 60 mL H_2O solution containing 0.8 g NaOH. The mixture stirred at room temperature for 30 min was then transferred into 100 mL Teflon-lined stainless steel autoclave and maintained at 150 °C for 12 h. After natural cooling, the obtained mixture was collected by centrifugation at 7000 rpm for 2 min. The obtained green powder was washed several times with water, DMF and methanol respectively, and dried at 100 °C overnight. Then, the activated NH_2-MIL-101(Cr) was obtained.

2.2.2. Preparation of Salicylaldehyde-NH_2-MIL-101(Cr)

To modify NH_2-MIL-101(Cr) with salicylaldehyde, 0.40 g of NH_2-MIL-101(Cr) was first dispersed into 30 mL of methanol in a flask under ultrasound, and 0.62 mL of salicylaldehyde was then added to the mixture, then the solution was refluxed at 85 °C for 10 h. Afterwards, the precipitate was washed with abundant ethanol three times and dried under vacuum at 40 °C overnight. The obtained product was Salicylaldehyde-NH_2-MIL-101(Cr) by the reaction as shown in Scheme 1, which we labeled as LP.

2.2.3. Preparation of TiO_2@Salicylaldehyde-NH_2-MIL-101(Cr)

The synthesis of TiO_2@Salicylaldehyde-NH_2-MIL-101(Cr) was the same as that of Salicylaldehyde-NH_2-MIL-101(Cr) (LP) but adding additional 0.505 mL tetrabutyl titanate into mixture of NH_2-MIL-101(Cr) and salicylaldehyde during synthesis. The obtained grass green product was named as TiO_2@Salicylaldehyde-NH_2-MIL-101(Cr), which was labeled as LP(Ti). For comparison, TiO_2@NH_2-MIL-101(Cr) was synthesized with the same method above.

2.3. Characterization

The powder X-ray diffraction (PXRD) measurements were recorded on a Bruker D8 Advance diffractometer with monochromatized Cu Kα radiation (λ = 0.15418 nm) source at 40 kV and 40 mA. The morphologies of the as-prepared samples were observed by transmission electron microscopy (TEM). The elemental composition of the samples were characterized by energy-dispersive X-ray spectroscopy (EDS, Oxford instruments X-Max). The chemical compositions were analysed by inductively coupled plasma-atomic emission spectrometry (ICP-AES, Varian 715-ES) and X-ray photoelectron spectroscopy (XPS, ESCALAB 250Xi). The Fourier transform infrared (FTIR) spectroscopy was recorded on Nicolet 6700 FTIR Spectrometric Analyzer using KBr pellets. UV–vis diffused reflectance spectra of the samples were obtained for the dry-pressed film samples using a UV–vis spectrophotometer (UV-3600, Shimadzu, Japan). $BaSO_4$ was used as a reflectance standard in a UV–vis diffuse reflectance experiment. The Brunauer–Emmett–Teller (BET) surface area and porous structure were measured using an ASAP 2460 V2.01 apparatus (Micromeritics Instrument Corp., USA). After the samples were

degassed in vacuum at 150 °C for 6 h, the nitrogen adsorption and desorption isotherms were measured at 77 K.

2.4. Photocatalytic degradation experiments

The photocatalytic activities of LP and LP(Ti) photocatalysts were evaluated by the photodegradation of MB dye under a 500 W Xe lamp irradiation in open air and at room temperature. The distance between the light source and the reactor containing reaction mixture was fixed at 15 cm. Typically, 0.005 g photocatalyst sample was added into 40 mL of MB aqueous solution (30 mg/L) in a 50 mL cylindrical Pyrex vessel reactor. The pH value of the suspension was adjusted to neutral (pH = 7.0). Prior to irradiation, the suspension was magnetically stirred in dark for 12 h to establish the adsorption/desorption equilibrium, followed by the addition of a known concentration of H_2O_2 to the mixture solution. During the photodegradation reaction, stirring was maintained to keep the mixture in suspension. Samples were withdrawn at regular intervals and immediately centrifuged to separate photocatalysts for analysis. To measure the photocatalytic activity under visible irradiation, a 420 nm UV-cutoff filter was used to provide the visible light.

2.5. Analytical methods

The MB concentration was monitored by measuring the absorption intensity at its maximum absorbance wavelength of λ = 664 nm using a UV–vis spectrophotometer (UV-3600, Shimadzu) in a 1 cm path length spectrometric quartz cell. The pH of MB solution was adjusted by adding aqueous solutions of 0.1 mol L^{-1} HCl or 0.1 mol L^{-1} NaOH, and determined by using a PHS-3C pH meter (Rex Instrument Factory, Shanghai, China). The formation of hydroxyl radicals (•OH) mediated by LP and LP(Ti) photocatalysts in the presence of H_2O_2 was detected by fluorescence method using terephthalic acid as a probe molecule [24]. The experimental procedures were similar to those used in the measurement of above catalytic experiments in the presence of H_2O_2 under visible light irradiation except that the aqueous solution of MB was replaced by an aqueous solution of 0.5 mM terephthalic acid and 2 mM NaOH. The visible light irradiation was continuous and sampling was performed every 15 min for analysis with a RF-5301PC Shimadzu fluorescence spectrophotometer at 315 nm of excitation wavelength.

2.6. Electrochemical measurements

An electrochemical work station (CHI660D Instruments) connected to a computer was used in our electrochemical experiment. The electrodes were prepared according to Zhang's method [25]. For the preparation of the MOF electrodes, the photocatalysts were dispersed in chitosan solution to form a 10 mg mL^{-1} solution and ultrasonicated for 5 min, 0.3 mL of colloidal solution was dropped on the pretreated ITO surface and allowed to dry under vacuum conditions for 24 h at room temperature. The photocurrents were measured by an electrochemical analyzer in a standard three electrode system with the LP(Ti) as the working electrodes, a Pt foil as the counter electrode, and a saturated calomel electrode (SCE) as a reference electrode. A 0.5 M Na_2SO_4 aqueous solution was used as the electrolyte. The Mott–Schottky measurements were carried out with impedance-potential model to evaluate the band positions of the LP(Ti) photocatalyst.

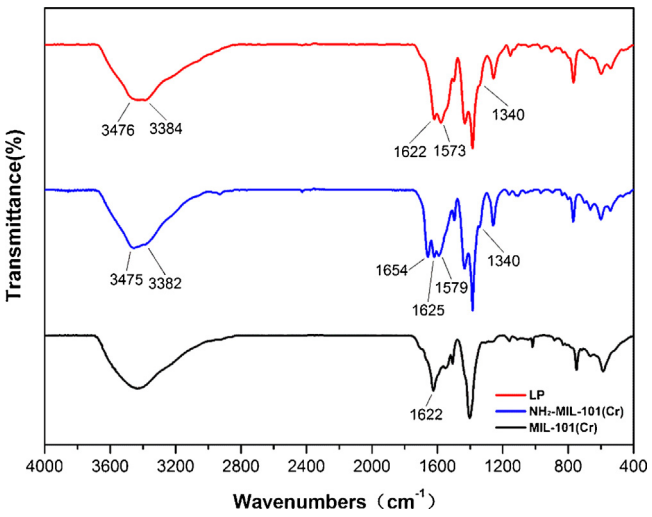

Fig. 1. FTIR spectra of LP, NH_2-MIL-101(Cr) and MIL-101(Cr).

3. Results and discussion

3.1. Characterization of the LP and LP(Ti)

In order to confirm that salicylaldehyde successfully reacted with NH_2-MIL-101(Cr), the FTIR spectra of LP referred to the parent NH_2-MIL-101(Cr) and MIL-101(Cr) samples were compared as shown in Fig. 1. Different from MIL-101(Cr), NH_2-MIL-101(Cr) showed a new IR peak at 1654 cm^{-1}, which was attributed to the bending vibration adsorption of the amino groups [26]. Moreover, a new tiny peak at 1340 cm^{-1} corresponded to the C—N stretching on benzene ring [23] can be noticed. Additionally, the double peaks at 3475 cm^{-1} and 3382 cm^{-1} can be assigned to asymmetric and symmetric vibration of the amino groups. The results suggested that the amino groups were successfully incorporated into MIL-101(Cr) forming NH_2-MIL-101(Cr). By further reacting NH_2-MIL-101(Cr) with salicylaldehyde, the resulting LP showed a decreased relative intensities of double peaks at 3475 cm^{-1} and 3382 cm^{-1}. More importantly, the amino peak at 1654 cm^{-1} was noticed to disappear, suggesting the reaction between amino groups on NH_2-MIL-101(Cr) with the added linking agent salicylaldehyde occurred, which caused the elongation of conjugated chain length of LP as demonstrated in Scheme 1.

X-ray powder diffraction (XRD) patterns of NH_2-MIL-101(Cr), TiO_2@NH_2-MIL-101(Cr), LP and LP(Ti) are shown in Fig. 2. The diffraction peaks of the NH_2-MIL-101(Cr) were in good agreement with those reported previously [23], indicating the successful synthesis of NH_2-MIL-101(Cr). Referred to the base NH_2-MIL-101(Cr), TiO_2@NH_2-MIL-101(Cr), LP and LP(Ti) showed similar XRD patterns, suggesting the crystal structure of NH_2-MIL-101(Cr) remained intact after covalently bonding salicylaldehyde and loading TiO_2. It further suggested that the NH_2-MIL-101(Cr) can act as a stable and tunable matrix for the incorporation of versatile functionalities. It should be noted that no characteristic peaks were observed for crystalline titanium dioxide in the LP(Ti) patterns, which may be due to the limitation of XRD technique to detect smaller nanoparticles. The result also suggested TiO_2 was homogeneously distributed in the framework of LP(Ti) [27], which was further confirmed by the EDS elemental mapping (Fig. 3).

Fig. 4 shows nitrogen adsorption-desorption isotherms of the samples. All the four samples displayed the same type I isotherms according to the IUPAC classification, indicating that there are mainly micropores in the samples. However, it was also observed that there were small indistinct hysteresis loop, which is associated with capillary condensation taking place in a small number of

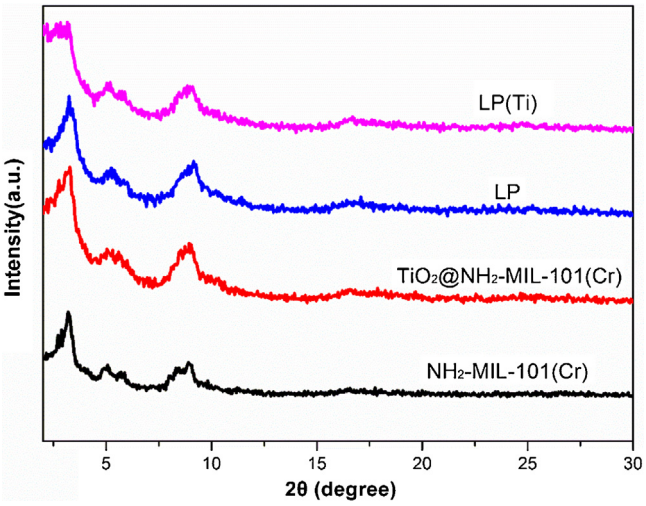

Fig. 2. Power XRD patterns of NH_2-MIL-101(Cr), TiO_2@NH_2-MIL-101(Cr), LP and LP(Ti).

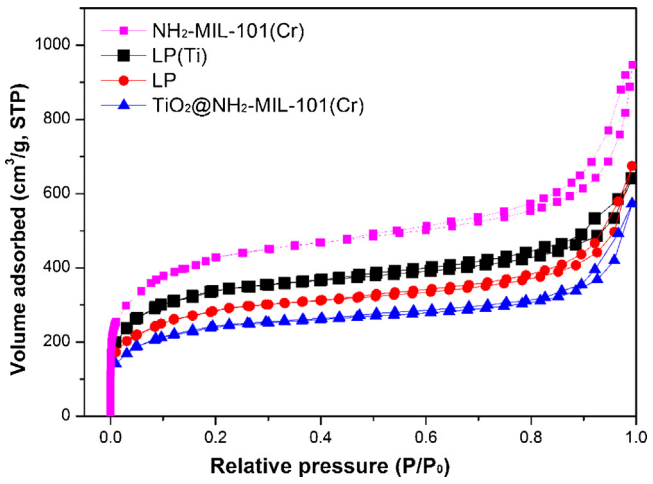

Fig. 4. Nitrogen adsorption-desorption isotherms of NH_2-MIL-101(Cr), TiO_2@NH_2-MIL-101(Cr), LP and LP(Ti) at 77 K.

mesopores, implying existence of a little of mesopores [28]. The similar behaviors of the samples suggested that the pore structure of NH_2-MIL-101(Cr) was well reserved after modification. The Brunauer–Emmet–Teller(BET) surface area and total pore volume are listed in Table 1. The BET surface area of NH_2-MIL-101(Cr), LP and LP(Ti) samples was 1506.6, 1190.1 and 853.0 $m^2\ g^{-1}$, respectively, decreasing in the order of NH_2-MIL-101(Cr) > LP > LP(Ti). The same trend was also observed on the total pore volume. Referred to the parent NH_2-MIL-101(Cr), the decreased surface area and

Table 1
BET surface area and pore volume of NH_2-MIL-101(Cr), TiO_2@NH_2-MIL-101(Cr), LP and LP(Ti).

Samples	S_{BET} ($m^2\ g^{-1}$)	Total pore volume ($cm^3\ g^{-1}$)
NH_2-MIL-101(Cr)	1523	0.23
TiO_2@NH_2-MIL-101(Cr)	1005	0.13
LP	1190	0.20
LP(Ti)	853	0.12

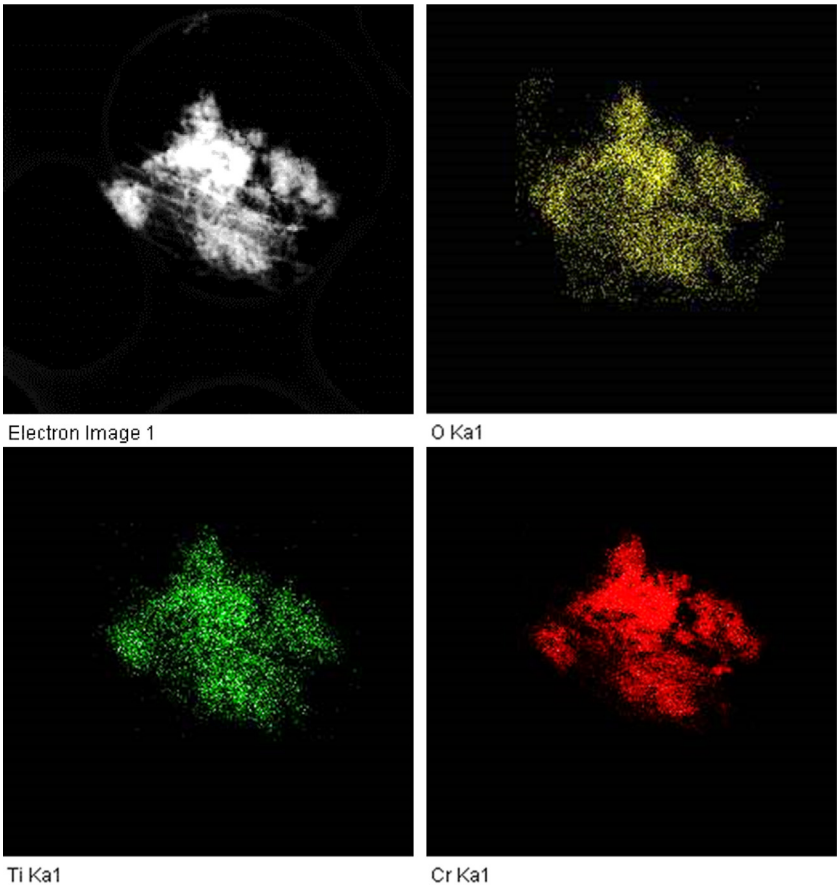

Fig. 3. EDS element mappings (O, Ti and Cr) of LP(Ti).

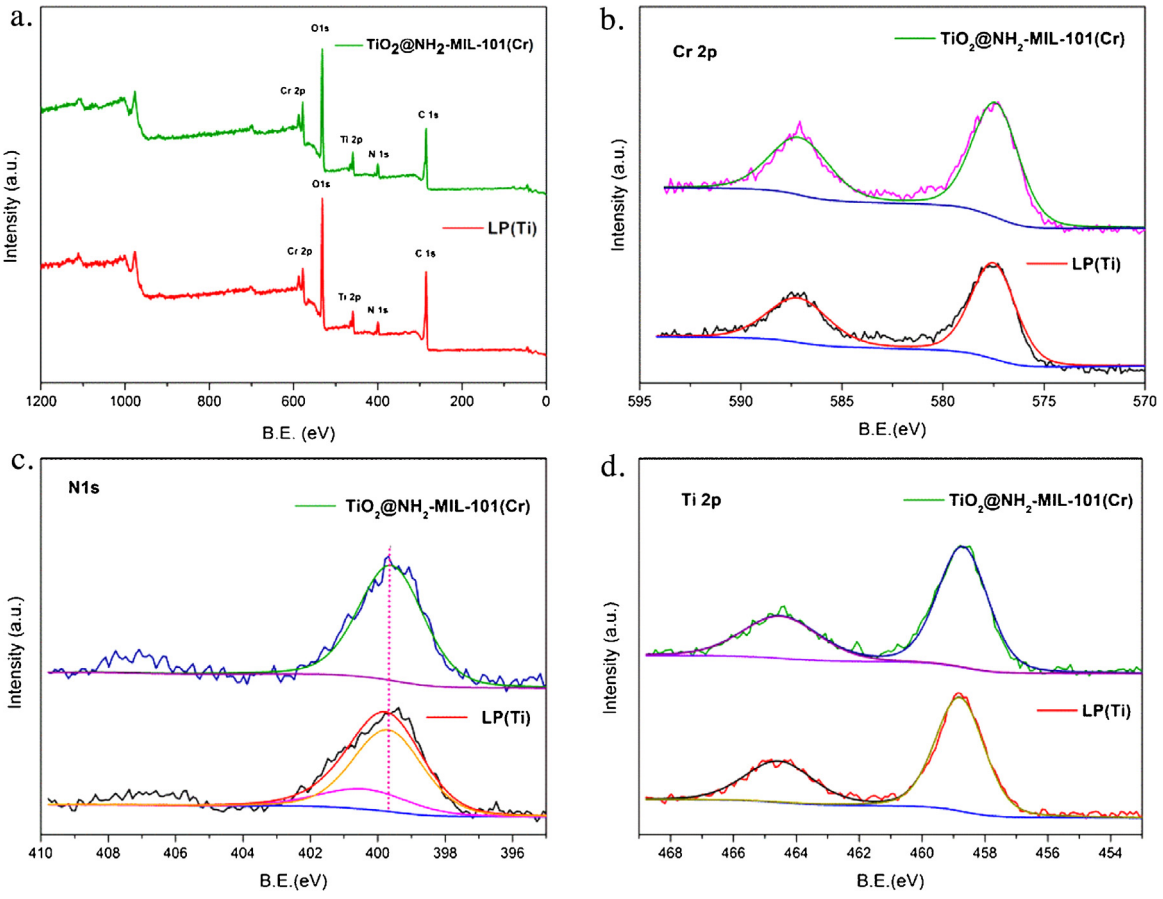

Fig. 5. X-ray photoelectron spectra of (a) the LP(Ti) and TiO_2@NH_2-MIL-101(Cr), (b) Cr 2p, (c) N 1s and (d) Ti 2p.

pore volume of LP can be due to the partial occupation of pores in NH_2-MIL-101(Cr) by the introduced covalently bonded phenol group inside the pores. This was further verified by the smaller surface area and pore volume of LP(Ti) than TiO_2@NH_2-MIL-101(Cr) (Table 1) without the introduction of covalently bonded phenol group in the NH_2-MIL-101(Cr) support, though the TiO_2 loading were almost the same (0.51 and 0.50 mmol g^{-1} for TiO_2@NH_2-MIL-101(Cr) and LP(Ti), respectively measured by ICP-AES). Referred to LP, the decreased surface area and pore volume of LP(Ti) suggested that TiO_2 was successfully loaded into the pores of LP.

XPS was employed to gain insight on the surface composition and the chemical environment of the LP(Ti) and TiO_2@NH_2-MIL-101(Cr). The spectrum in Fig. 5a shows that both samples were comprised of C, O, Cr, N and Ti. As shown in Fig. 5b, the Cr $2p_{1/2}$ and Cr $2p_{3/2}$ peaks located at 587.2 and 577.6 eV suggested the existence of Cr—O, consistent with the literature values [29]. Fig. 5c presents the XPS spectrum of N 1s, which can be resolved to two peaks at 400.6 and 399.9 eV for LP(Ti), characteristic of imine groups [30] and amino groups [26], respectively, while only one peak at 399.8 eV was found for TiO_2@NH_2-MIL-101(Cr), corresponding to amino group [26]. The result further confirmed the reaction between salicylaldehyde and NH_2-MIL-101(Cr) occurred. The Ti 2p XPS spectra was shown in Fig. 5d. The Ti $2p_{3/2}$ and Ti $2p_{1/2}$ core level peaks appeared at the binding energies of 458.8 and 464.6 eV, respectively, which was contributed by the O—Ti—O bonding in TiO_2 [31–33]. The analysis confirmed the titanic species loaded on LP(Ti) and TiO_2@NH_2-MIL-101(Cr) were TiO_2.

UV–vis diffuse reflectance spectra (DRS) were employed to characterize the optical properties of the samples. As shown in Fig. 6, the absorption-band positions of NH_2-MIL-101(Cr), TiO_2@NH_2-MIL-101(Cr), LP and LP(Ti) in the UV region are ascribed to π–π^*

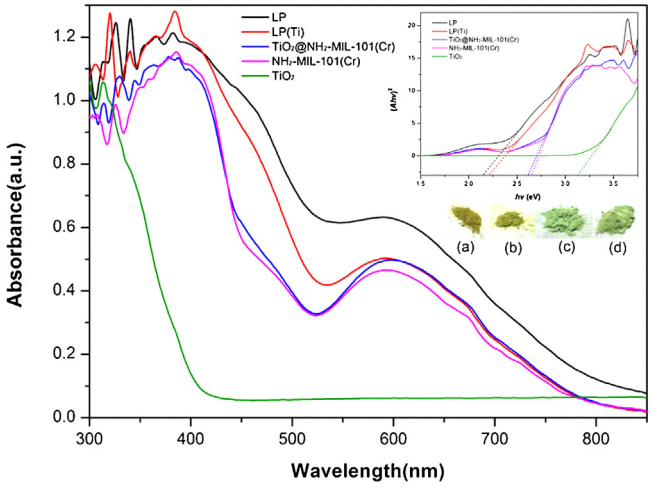

Fig. 6. UV–vis DRS spectra and plots of $(Ahv)^2$ vs. photon energy of NH_2-MIL-101(Cr), TiO_2@NH_2-MIL-101(Cr), LP, LP(Ti) and TiO_2; photographs of (a) LP, (b) LP(Ti), (c) TiO_2@NH_2-MIL-101(Cr), and (d) NH_2-MIL-101(Cr) are presented in the inset.

transitions of ligands [34], whereas the absorption band around 600 nm belongs to d–d spin-allowed transition of Cr^{3+} centers [35]. The absorption of pure TiO_2 at wavelengths shorter than 400 nm can be assigned to the band gap of TiO_2. Furthermore, the photographs of the four NH_2-MIL-101(Cr)-based samples were shown in the inset of Fig. 6. The colors of the four samples were different, whose color change from (d) to (a) suggested that the light absorption intensity in the visible region increased after modifying

NH_2-MIL-101(Cr) with salicylaldehyde, which may be attributed to the elongated conjugated aromatic structure in LP. Therefore, compared with NH_2-MIL-101(Cr), LP showed enhanced absorbance in the visible light region (>500 nm). On the other hand, the band-gap energy can be estimated from the intercept of the tangents of $(Ahv)^2$ vs. photon energy [36]. The inset of Fig. 6 presents the intercepts of the tangents of $(Ahv)^2$ vs. photon energy for five samples. Thus, the band-gap values of these samples were estimated from these intercepts to be about 2.15, 2.21, 2.62, 2.65 and 3.20 eV for LP, LP(Ti), TiO_2@NH_2-MIL-101(Cr), NH_2-MIL-101(Cr) and TiO_2, respectively. It indicated that the introduction of salicylaldehyde significantly enhanced the light-absorption properties of LP and LP(Ti), undergoing redshift compared with NH_2-MIL-101(Cr) and TiO_2@NH_2-MIL-101. Meanwhile, for LP and LP(Ti), the almost the same band-gap energy indicates that the TiO_2 encapsulated in Salicylaldehyde-NH_2-MIL-101(Cr) had not destroyed the framework, which is expected that LP with excellent optical properties in UV–vis region may provide a good platform for accommodating TiO_2 to achieve excellent photocatalytic properties.

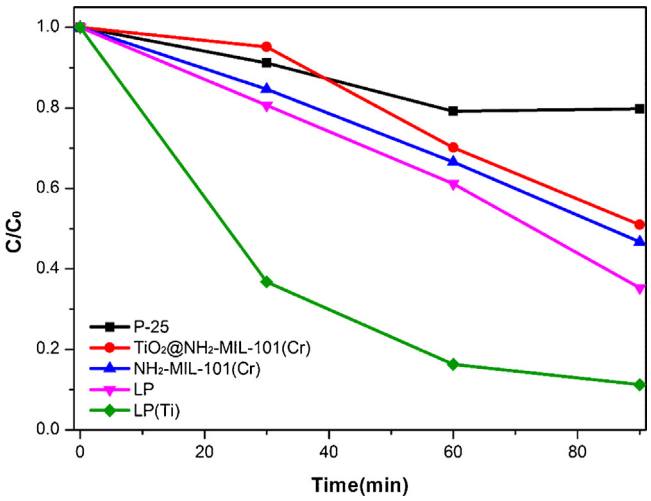

Fig. 7. Degradation efficiency of MB over the NH_2-MIL-101(Cr), TiO_2@NH_2-MIL-101(Cr), LP, LP(Ti) and P-25 (TiO_2) under visible light. (Reaction conditions: 5 mg of photocatalyst, 40 mL of 30 mg/L MB, 100 μL of H_2O_2, pH of 7).

3.2. MB photodegradation of the LP(Ti)

The photocatalytic activity was evaluated in the photocatalytic degradation of aqueous MB under visible-light irradiation. Fig. 7 shows the degradation efficiency of MB over NH_2-MIL-101(Cr), TiO_2@NH_2-MIL-101(Cr), LP, LP(Ti) and Degussa P-25 under visible-light. LP(Ti) achieved the highest MB degradation (86% degradation in 60 min of visible-light irradiation) among the tested samples, suggesting LP(Ti) can be a new highly active MOF-based complex photocatalyst for MB photodegradation under visible light. Importantly, though TiO_2 loading in LP(Ti) and TiO_2@NH_2-MIL-101(Cr) was almost the same (0.51 and 0.50 mmol g^{-1} for TiO_2@NH_2-MIL-101(Cr) and LP(Ti), respectively), the BET surface area of TiO_2@NH_2-MIL-101(Cr) was even higher than LP(Ti) (1005 and 853 m^2 g^{-1} for TiO_2@NH_2-MIL-101(Cr) and LP(Ti), respectively), LP(Ti) showed tripled degradation efficiency of MB of TiO_2@NH_2-MIL-101(Cr), suggesting the modification of NH_2-MIL-101(Cr) with

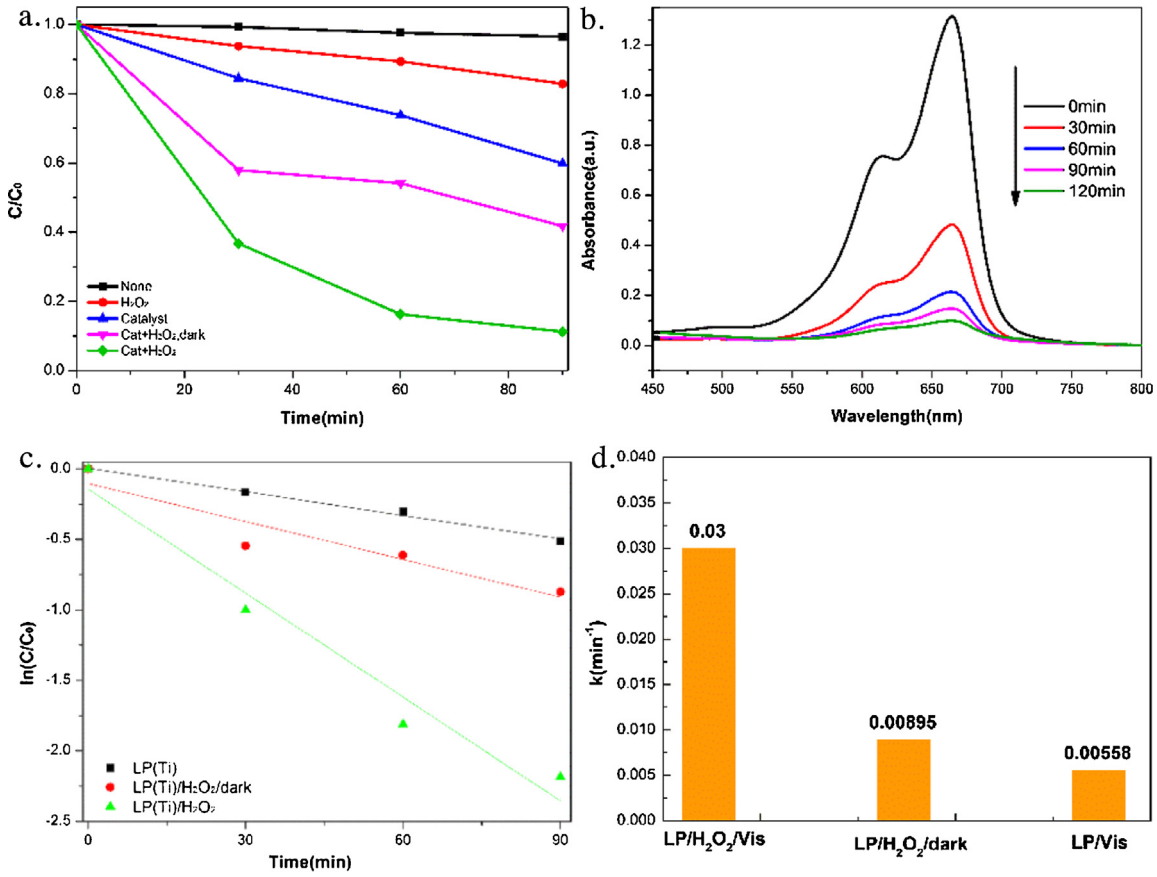

Fig. 8. (a) Degradation efficiency of MB under different conditions. (b) The UV–vis spectral changes of MB with time. (c) Pseudo-first-order kinetics curves of the degradation of MB under different conditions. (d) Comparison of the apparent reaction rate constants of the degradation of MB under different conditions. (Reaction conditions: 5 mg photocatalyst, 40 mL of MB at 30 mg/L, 100 μL of H_2O_2, pH of 7).

salicylaldehyde had pronounced effect on MB photodegradation. It also hinted that the modification of stable MOF matrix with elongated conjugation linker to encapsulate metal oxides can be a new strategy to design effective visible light-induced MOF-based composite photocatalysts and worthy of further exploration in the future.

Control experiments were conducted to verify the photodegradation performance of LP(Ti). Fig. 8a shows the variation of MB concentration (C/C_0) with time under different systems. After visible light irradiation for 90 min, the concentration of MB keep almost the same without LP(Ti) and H_2O_2, indicating that the MB did not go through self-decomposition under visible light irradiation. After adding H_2O_2, the degradation efficiency of MB reached 15% at 90 min, which was attributed to the photolysis of H_2O_2 under visible irradiation and produced •OH. When LP(Ti) existed alone under visible light without H_2O_2, 40% degradation efficiency of MB was reached at 90 min, suggesting the LP(Ti) itself possessed photoreactivity to some extent. What's more, in the presence of LP(Ti) and H_2O_2 under dark condition, almost 60% of degradation efficiency of MB was reached after 90 min, indicating the synergetic effect of LP(Ti) and H_2O_2 was present on MB degradation. Amazingly, in the presence of LP(Ti) and H_2O_2 under visible light, almost 90% degradation efficiency of MB was observed after 90 min, and then the concentration varied slowly, mainly due to the adsorption-desorption equilibrium of MB. Few MB desorbed from LP(Ti) surface, which resulted in the very slow degradation rate in the final stage. The UV–vis absorption spectral change of the MB in the presence of LP(Ti) and H_2O_2 under visible light with time was shown in Fig. 8b, proving the strong photocatalytic activity of LP(Ti) with H_2O_2.

The linear plot of $\ln(C/C_0)$ vs. reaction time t was shown in Fig. 8c. The kinetic data for the degradation of MB was fitted by the pseudo-first-order rate equation, with the rate constants presented in Fig. 8d. The rate constant of the LP(Ti)/visible light/H_2O_2 system (0.03 min^{-1}) tripled that of the LP(Ti)/dark/H_2O_2 system (0.00895 min^{-1}), indicating visible light played an important role for the dramatically enhanced photodegradation kinetics of the LP(Ti). In order to evaluate the synergetic effect in the LP(Ti)/visible light/H_2O_2 system, the parameter of synergetic index (SI) was introduced, $SI = k_{MVH}/(k_{MH} + k_{MV})$, where k_{MVH}, k_{MV}, and k_{MH} were the apparent rate constants in the catalytic systems of LP(Ti)/visible light/H_2O_2, LP(Ti)/visible light and LP(Ti)/H_2O_2/dark, respectively [27]. The SI was calculated to be 2.06, indicating the synergistic effect of LP(Ti)/visible light/H_2O_2 was enhanced by 106%.

The effect of pH on the degradation efficiency of MB was investigated as shown in Fig. 9. The degradation rate of MB increased with the increase of pH from 3.0 to 9.0. This could be attributed to the fact that the adsorption of the cationic MB dye molecule can be affected by the co-present hydrion, as it could react with the carboxylate ions on the surface of LP(Ti) in an acidic solution (pH < 7). By further increasing pH from 9 to 11, the degradation rate of MB decreased, which was due to the decomposition of the unstable H_2O_2 in alkaline medium [37].

In order to evaluate the effects of the amount of H_2O_2, the degradation of MB at different amounts of H_2O_2 (40, 60, 100 and 120 μL) were compared as shown in Fig. 10. The degradation efficiency of MB increased with the added H_2O_2 amount from 40 to 100 μL. However, it decreased by further adding the amount of H_2O_2 to 120 μL, mainly due to the surplus H_2O_2 molecules act as the scavenger of •OH radicals. (Eqs. (1) and (2)).

$$H_2O_2 + {}^{\bullet}OH \rightarrow H_2O + HOO^{\bullet} \quad (1)$$

$$HOO^{\bullet} + {}^{\bullet}OH \rightarrow H_2O + O_2 \quad (2)$$

The reusability of LP(Ti) was evaluated in the circulating runs in catalytic degradation of MB over LP(Ti)/visble/H_2O_2 system as

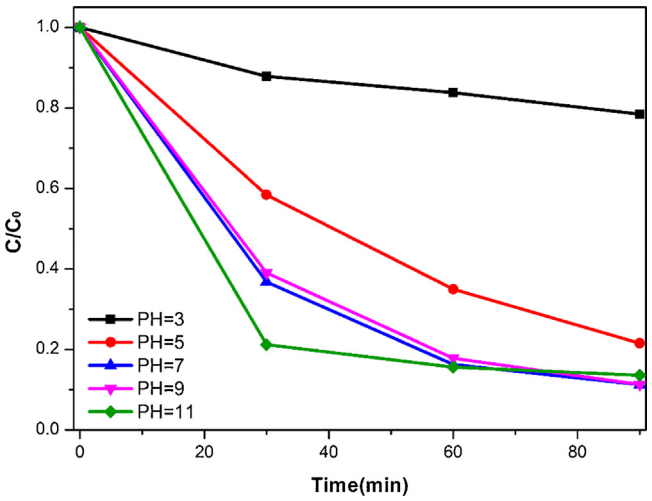

Fig. 9. Effect of initial pH on the degradation of MB. (Reaction conditions: 5 mg of photocatalyst, 40 mL of MB at 30 mg/L, 100 μL of H_2O_2, pH of 7).

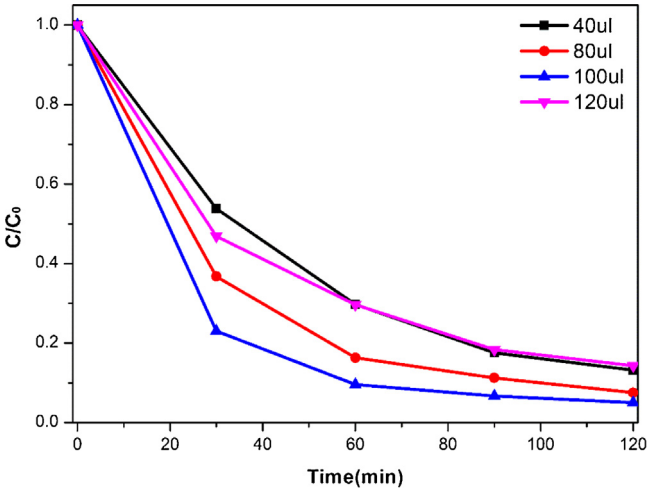

Fig. 10. Effect of H_2O_2 concentration on the degradation of MB over LP(Ti)/visible light/H_2O_2 system. (Reaction conditions: 5 mg of photocatalyst, 40 mL of MB at 30 mg/L, pH of 7).

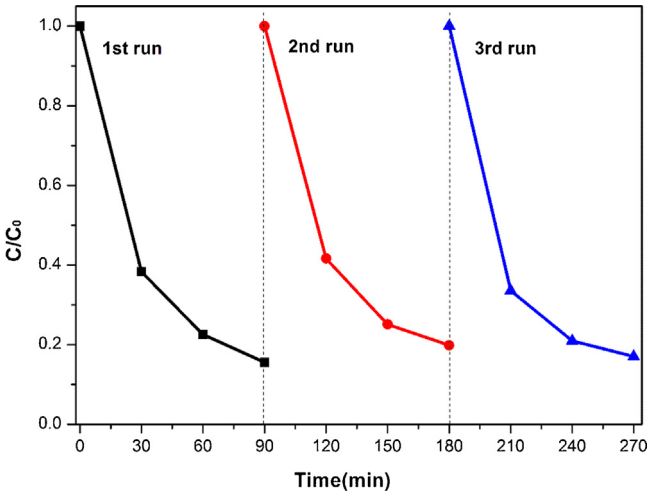

Fig. 11. The cycling runs of the degradation of MB (30 mg L^{-1}) over LP(Ti)/visible light/H_2O_2 system.

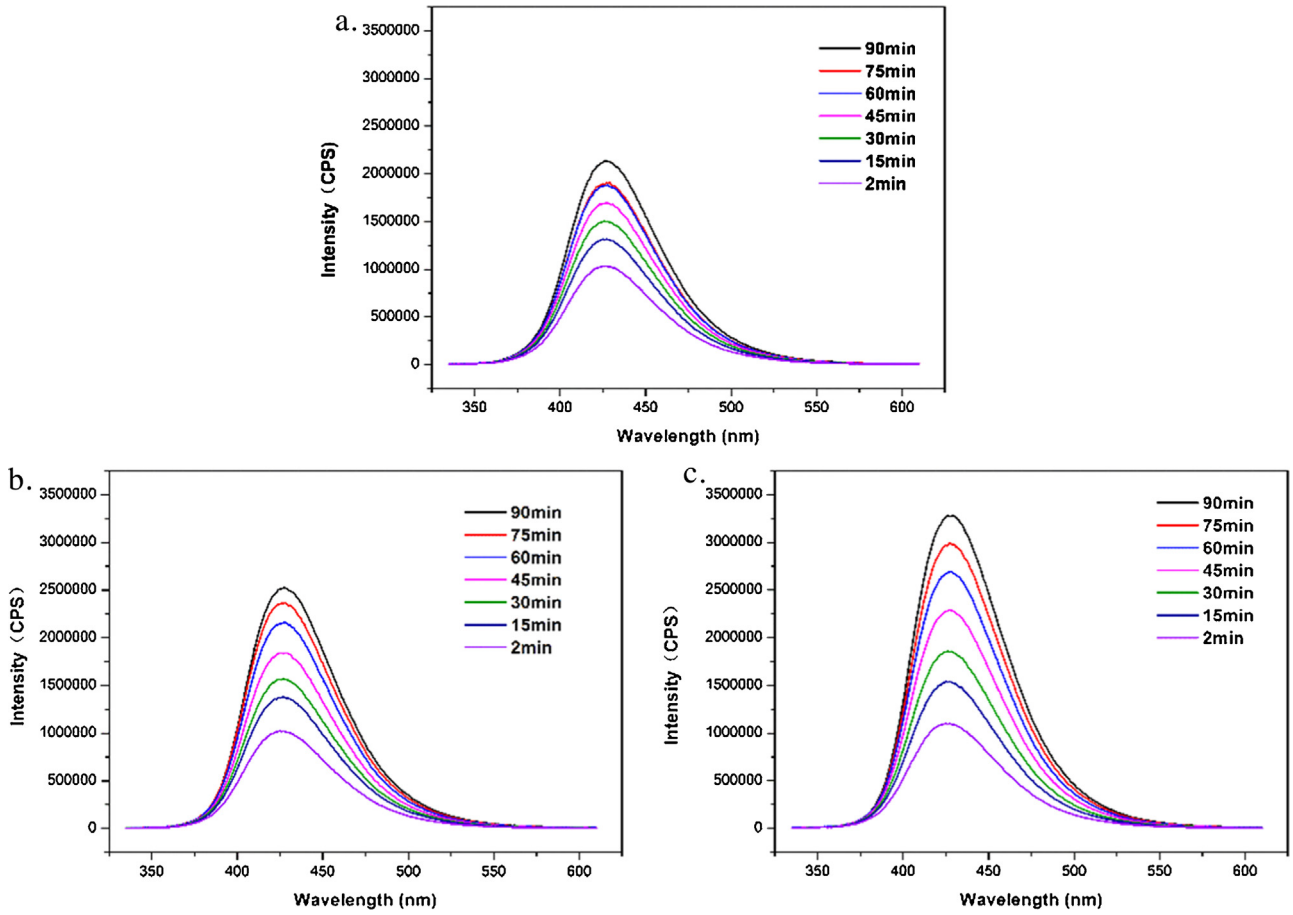

Fig. 12. PL spectra of different photocatalytic systems: (a) LP(Ti)/visible light, (b) LP(Ti)/H_2O_2 and (c) LP(Ti)/visible light/H_2O_2 using terephthalic acid as the probe molecule.

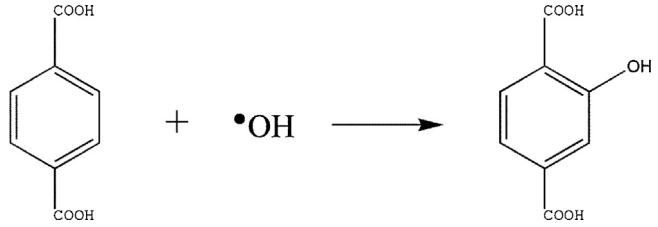

Scheme 2. Formation of 2-hydroxyterephthalic acid in the reaction of terephthalic acid with hydroxyl radicals.

shown in Fig. 11. The photocatalytic activities of LP(Ti) did not decrease after three cycles, indicating that the LP(Ti) photocatalyst exhibited great stability in this reaction system.

3.3. Mechanism for the MB degradation in LP(Ti)/visible/H_2O_2 system

The hydroxyl radicals plays a most important part in the degradation of MB [38]. Terephthalic acid was employed as a probe molecule (Scheme 2) to detect the hydroxyl radicals (•OH) [24,39,40] on the surface of LP(Ti). Fig. 12 shows the PL spectra of different photocatalytic systems. PL intensity increases gradually with irradiation time, suggesting the increase in the concentration of hydroxyl radicals formed at the surface of LP(Ti) under visible light irradiation with time. The strongest PL intensity was observed in the LP(Ti)/visible/H_2O_2 system, indicating the most hydroxyl radicals was generated, and thus contributed to the highest degradation efficiency of such system. Moreover, the result also suggested the synergistic effect between LP(Ti) and H_2O_2 under visible light.

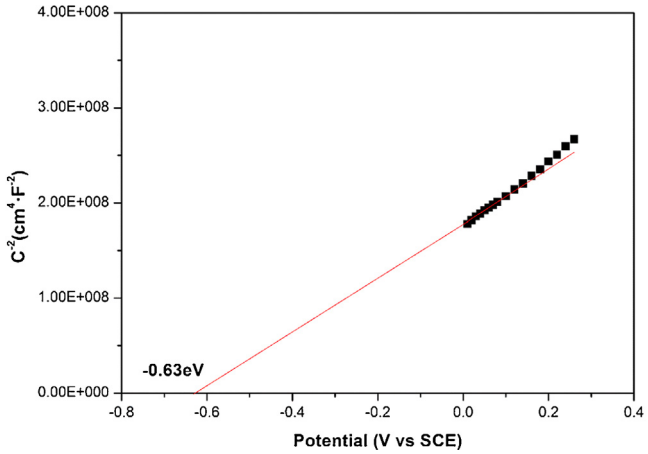

Fig. 13. Mott–Schottky plots for the LP electrode.

Mott–Schottky measurement of LP was performed to understand the intrinsic electronic properties [25] of LP(Ti). As shown in Fig. 13, the flat-band potential (V_{fb}) of the LP is −0.63 eV vs. SCE (corresponding to a potential of −0.39 vs. NHE). The conduction band (CB) of LP is estimated to −0.49 eV vs. NHE. With the band gap energy estimated from the UV–vis DRS spectrum (Fig. 6), the VB of LP was 1.66 eV vs. NHE according to the empirical formula $E_{CB} = E_{VB} - Eg$. The conduction band (CB) and the valance band (VB) of TiO_2 was −0.4 and 2.8 eV, respectively [41,42]. With these data,

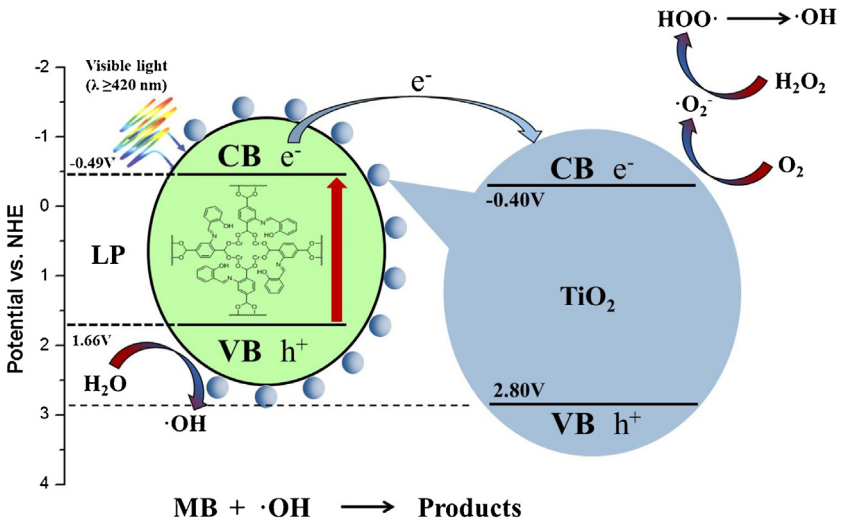

Fig. 14. Schematic illustration of the degradation of MB on LP(Ti) with H_2O_2 under visible light.

the degradation of MB using LP(Ti) with H_2O_2 under visible light was illustrated in Fig. 14. Under visible light irradiation, the electron of LP transfers from the VB to the CB. Then the excited electron of LP transfers to the CB of TiO_2, which could separate photogenerated hole-electron pairs efficiently [43,44]. In the LP(Ti)/visible light system without H_2O_2, the electron of TiO_2 reacts with the oxygen molecule from ambient air to form $^{\bullet}O_2^-$, which then transforms to the hydroxyl radicals, and the holes of LP left in VB oxidizes water to produce hydroxyl radicals. In contrast, the addition of H_2O_2 (the LP(Ti)/visible/H_2O_2 system) made it a more efficient process [45] as more paths were provided to generate hydroxyl radicals by adding H_2O_2. First, the additional H_2O_2 reacts with the excited electron to generate hydroxyl radicals (Eq. (3)). Second, the $^{\bullet}O_2^-$ could also oxidize H_2O_2 to form hydroxyl radicals (Eq. (4)). Third, H_2O_2 itself decomposes to hydroxyl radicals under visible light irradiation (Eq. (5)).

$$e_{CB}^- + H_2O_2 \rightarrow OH^- + {}^{\bullet}OH \quad (3)$$

$$^{\bullet}O_2^- + H_2O_2 \rightarrow OH^- + {}^{\bullet}OH + O_2 \quad (4)$$

$$H_2O_2 + hv \rightarrow 2{}^{\bullet}OH \quad (5)$$

4. Conclusion

In this work, TiO_2 encapsulated in Salicylaldehyde-NH_2-MIL-101(Cr) was successfully fabricated and studied systematically for photodegradation of MB under visible light. By the strategic modification of the stable NH_2-MIL-101(Cr) matrix with salicylaldehyde, the conjugated linker was elongated, and the resulting framework (LP) showed enhanced absorbance of visible light, while remained the stable crystalline structure and porosity of NH_2-MIL-101(Cr). TiO_2 encapsulated in Salicylaldehyde-NH_2-MIL-101 (namely LP(Ti)) shows effectiveness toward photocatalytic degradation of MB under visible light, in which the introduced phenol group in the NH_2-MIL-101(Cr) matrix showed a pronounced impact, resulting in dramatically enhanced MB degradation from 30% of TiO_2@NH_2-MIL-101(Cr) to 86% of LP(Ti). The LP(Ti)/visible/H_2O_2 system showed the enhanced synergy index by 106%. The photodegradation mechanism of the LP(Ti)/visible/H_2O_2 system was further illustrated. Under visible light irradiation, the electron of LP transfers from the VB to the CB. Then the excited electron of LP transfers to the CB of TiO_2, which could separate photogenerated hole-electron pairs efficiently. The high degradation efficiency, fast kinetics and excellent recycling stability made the LP(Ti)/visible/H_2O_2 system excel in the photodegradation of MB under visible light. This work provides a new approach using TiO_2@MOF for visible light-induced photodegradation of organic contaminants for the environmental remediation.

Acknowledgements

We gratefully acknowledge the research grants provided by the National Natural Science Foundation of China (21576093), Guangdong Natural Science Funds for Distinguished Young Scholar, Pearl River S&T Nova Program of Guangzhou, the Scientific Research Foundation for the Returned Overseas Chinese Scholars, State Education Ministry, and Fundamental Research Funds for the Central Universities.

References

[1] A. Mills, S.L. Hunte, An overview of semiconductor photocatalysis, J. Photochem. Photobiol. A: Chem. 108 (1997) 1–35.
[2] N.F. Steven, A.J. Bard, Heterogeneous photocatalytic oxidation of cyanide ion in aqueous solution at TiO_2 powder, J. Am. Chem. Soc. 99 (1977) 303–304.
[3] M.R. Hoffmann, S.T. Martin, W. Choi, D.W. Bahnemann, Environmental applications of semiconductor photocatalysis, Chem. Rev. 95 (1995) 69–96.
[4] T.L. Thompson, J.T. Yates Jr., Surface science studies of the photoactivation of TiO_2—new photochemical processes, Chem. Rev. 106 (2006) 4428–4453.
[5] U.G. Akpan, B.H. Hameed, Parameters affecting the photocatalytic degradation of dyes using TiO_2-based photocatalysts: a review, J. Hazard. Mater. 170 (2009) 520–529.
[6] K. Ayoub, E.D. van Hullebusch, M. Cassir, A. Bermond, Application of advanced oxidation processes for TNT removal: a review, J. Hazard. Mater. 178 (2010) 10–28.
[7] A.O. Kondrakov, A.N. Ignatev, V.V. Lunin, F.H. Frimmel, S. Bräse, H. Horn, Roles of water and dissolved oxygen in photocatalytic generation of free OH radicals in aqueous TiO_2 suspensions: an isotope labeling study, Appl. Catal. B: Environ. 182 (2016) 424–430.
[8] P. Horcajada, C. Serre, G. Maurin, N.A. Ramsahye, F. Balas, M. Vallet-Regí, M. Sebban, F. Taulelle, Flexible porous metal-organic frameworks for a controlled drug delivery, J. Am. Chem. Soc. 130 (2008) 6774.
[9] M. Alvaro, E. Carbonell, B. Ferrer, F.X. Llabres i Xamena, H. Garcia, Semiconductor behavior of a metal-organic framework (MOF), Chemistry 13 (2007) 5106–5112.
[10] T.R. Cook, Y.R. Zheng, P.J. Stang, Metal–organic frameworks and self-assembled supramolecular coordination complexes: comparing and contrasting the design, synthesis, and functionality of metal-organic materials, Chem. Rev. 113 (2013) 734–777.
[11] C.D. Wu, A.G. Hu, L. Zhang, W.B. Lin, A homochiral porous metal-Organic framework for highly enantioselective heterogeneous asymmetric catalysis, J. Am. Chem. Soc. 127 (2005) 8940.
[12] Y. Qi, Y. Luan, J. Yu, X. Peng, G. Wang, Nanoscaled copper metal-organic framework (MOF) based on carboxylate ligands as an efficient heterogeneous catalyst for aerobic epoxidation of olefins and oxidation of benzylic and allylic alcohols, Chemistry 21 (2015) 1589–1597.

[13] A. Dhakshinamoorthy, M. Alvaro, H. Garcia, Metal–organic frameworks as heterogeneous catalysts for oxidation reactions, Catal. Sci. Technol 1 (2011) 856.
[14] A. Dhakshinamoorthy, M. Alvaro, H. Garcia, Commercial metal–organic frameworks as heterogeneous catalysts, Chem. Commun. 48 (2012) 11275–11288.
[15] X.L.X. Francesc, A. Corma, H. Garcia, Applications for metal–organic frameworks (MOFs) as quantum dot semiconductors, J. Phys. Chem. C 111 (2007) 80–85.
[16] Y. Luan, N. Zheng, Y. Qi, J. Tang, G. Wang, Merging metal–organic framework catalysis with organocatalysis: a thiourea functionalized heterogeneous catalyst at the nanoscale, Catal. Sci. Technol. 4 (2014) 925.
[17] Z. Wang, S.M. Cohen, Postsynthetic modification of metal–organic frameworks, Chem. Soc. Rev. 38 (2009) 1315–1329.
[18] Y. Luan, N. Zheng, Y. Qi, J. Yu, G. Wang, Development of a SO_3H-functionalized UiO-66 metal–organic framework by postsynthetic modification and studies of its catalytic activities, Eur. J. Inorg. Chem. 2014 (2014) 4268–4272.
[19] G. Férey, C. Mellot-Draznieks, C. Serre, F. Millange, J. Dutour, S. Surblé, I. Margiolaki, A chromium terephthalate-based solid with unusually large pore volumes and surface area, Science 309 (2005) 2040.
[20] S. Bernt, V. Guillerm, C. Serre, N. Stock, Direct covalent post-synthetic chemical modification of Cr-MIL-101 using nitrating acid, Chem. Commun. 47 (2011) 2838–2840.
[21] Y. Huang, S. Liu, Z. Lin, W. Li, X. Li, R. Cao, Facile synthesis of palladium nanoparticles encapsulated in amine-functionalized mesoporous metal–organic frameworks and catalytic for dehalogenation of aryl chlorides, J. Catal. 292 (2012) 111–117.
[22] X.W. Dong, T. Liu, Y.Z. Hu, X.Y. Liu, C.M. Che, Urea postmodified in a metal-organic framework as a catalytically active hydrogen-bond-donating heterogeneous catalyst, Chem. Commun. 49 (2013) 7681–7683.
[23] Y. Lin, C. Kong, L. Chen, Direct synthesis of amine-functionalized MIL-101(Cr) nanoparticles and application for CO_2 capture, RSC Adv. 2 (2012) 6417.
[24] K. Ishibashi, A. Fujishima, T. Watanabe, K. Hashimoto, Detection of active oxidative species in TiO_2 photocatalysis using the fluorescence technique, Electrochem. Commun. 2 (2000) 207–210.
[25] K. Zhao, X. Zhang, L. Zhang, The first BiOI-based solar cells, Electrochem. Commun. 11 (2009) 612–615.
[26] J. Wang, M. Yang, W. Dong, Z. Jin, J. Tang, S. Fan, Y. Lu, G. Wang, Co(ii) complexes loaded into metal–organic frameworks as efficient heterogeneous catalysts for aerobic epoxidation of olefins, Catal. Sci. Technol. 6 (2016) 161–168.
[27] L. Ai, C. Zhang, L. Li, J. Jiang, Iron terephthalate metal–organic framework: revealing the effective activation of hydrogen peroxide for the degradation of organic dye under visible light irradiation, Appl. Catal. B: Environ. 148–149 (2014) 191–200.
[28] L. Peng, J. Zhang, J. Li, B. Han, Z. Xue, G. Yang, Surfactant-directed assembly of mesoporous metal–organic framework nanoplates in ionic liquids, Chem. Commun. 48 (2012) 8688–8690.
[29] H. Khajavi, H.A. Stil, H.P.C.E. Kuipers, J. Gascon, F. Kapteijn, Shape and transition state selective hydrogenations using egg-shell Pt-MIL-101(Cr) catalyst, ACS Catal. 3 (2013) 2617–2626.
[30] H.J. Kim, I.S. Bae, S.J. Cho, J.H. Boo, B.C. Lee, J. Heo, I. Chung, B. Hong, Synthesis, structure, and photovoltaic property of a nanocrystalline 2H perovskite-type novel sensitizer $(CH_3CH_2NH_3)PbI_3$, Nanoscale Res. Lett. 7 (2012) 1–7.
[31] X.B. Chen, C. Burda, Photoelectron spectroscopic investigation of nitrogen-doped titania nanoparticles, J. Phys. Chem. B 108 (2004) 15446–15449.
[32] M.-S. Wong, H. Pang Chou, T.-S. Yang, Reactively sputtered N-doped titanium oxide films as visible-light photocatalyst, Thin Solid Films 494 (2006) 244–249.
[33] F. Peng, L. Cai, H. Yu, H. Wang, J. Yang, Synthesis and characterization of substitutional and interstitial nitrogen-doped titanium dioxides with visible light photocatalytic activity, J. Solid State Chem. 181 (2008) 130–136.
[34] M. Wen, K. Mori, T. Kamegawa, H. Yamashita, Amine-functionalized MIL-101(Cr) with imbedded platinum nanoparticles as a durable photocatalyst for hydrogen production from water, Chem. Commun. 50 (2014) 11645–11648.
[35] J. He, Z. Yan, J. Wang, J. Xie, L. Jiang, Y. Shi, F. Yuan, F. Yu, Y. Sun, Significantly enhanced photocatalytic hydrogen evolution under visible light over CdS embedded on metal–organic frameworks, Chem. Commun. 49 (2013) 6761–6763.
[36] F. Dong, L. Wu, Y. Sun, M. Fu, Z. Wu, S.C. Lee, Efficient synthesis of polymericg-C_3N_4 layered materials as novel efficient visible light driven photocatalysts, J. Mater. Chem. 21 (2011) 15171–15174.
[37] S. Zhang, X. Zhao, H. Niu, Y. Shi, Y. Cai, G. Jiang, Superparamagnetic Fe_3O_4 nanoparticles as catalysts for the catalytic oxidation of phenolic and aniline compounds, J. Hazard. Mater. 167 (2009) 560–566.
[38] Y. Ahmed, Z. Yaakob, P. Akhtar, Degradation and mineralization of methylene blue using a heterogeneous photo-Fenton catalyst under visible and solar light irradiation, Catal. Sci. Technol. 6 (2016) 1222–1232.
[39] Q. Xiao, Z. Si, J. Zhang, C. Xiao, X. Tan, Photoinduced hydroxyl radical and photocatalytic activity of samarium-doped TiO_2 nanocrystalline, J. Hazard. Mater. 150 (2008) 62–67.
[40] J.G. Yu, W.G. Wang, B. Cheng, B.L. Su, Enhancement of photocatalytic activity of mesporous TiO_2 powders by hydrothermal, J. Phys. Chem. C 113 (2009) 6743–6750.
[41] S. Linic, P. Christopher, D.B. Ingram, Plasmonic-metal nanostructures for efficient conversion of solar to chemical energy, Nat. Mater. 10 (2011) 911–921.
[42] O. Rosseler, M.V. Shankar, M.K.-L. Du, L. Schmidlin, N. Keller, V. Keller, Solar light photocatalytic hydrogen production from water over Pt and Au/TiO_2(anatase/rutile) photocatalysts: influence of noble metal and porogen promotion, J. Catal. 269 (2010) 179–190.
[43] G.K.C. Low, S.R. Mcevoy, R.W. Matthews, Formation of nitrate and ammonium ions in titanium dioxide mediated photocatalytic degradation of organic compounds containing nitrogen atoms, Environ. Sci. Technol. 25 (1991) 460–467.
[44] D.D. Dionysiou, M.T. Suidan, E. Bekou, I. Baudin, J.M. Laine, Effect of ionic strength and hydrogen peroxide on the photocatalytic degradation of 4-chlorobenzoic acid in water, Appl. Catal. B: Environ. 26 (2000) 153–171.
[45] L. Wen, J. Zhao, K. Lv, Y. Wu, K. Deng, X. Leng, D. Li, Visible-light-driven photocatalysts of metal–organic frameworks derived from multi-carboxylic acid and imidazole-based spacer, Cryst. Growth Des. 12 (2012) 1603–1612.